Dynamic Fracture Analysis of AISI 1020 Steel Tube under Internal Explosive Loading

Li Ma, Yang Hu , Yang Du, Jinyang Zheng

Institute of Process Equipment, Zhejiang University

Hangzhou, Zhejiang, P.R. China

1. Introduction

Explosion containment vessels (ECV) have become one of necessary equipments in the field of detonation physics, blast processing and anti-terrorism, etc. So far, several design methods of ECV have been presented such as British AWE design method [1] and ASME Code Case 2564-2[2], etc., where the fracture mechanics analysis is required to conduct to prevent brittle fracture. However considering dynamic load condition of ECV, whose strain rate may reach to 10^1 ~10^6 s^{-1}. Many researches have found when the loading rate exceeds a high certain value, material exhibits failure modes transition from brittle to ductile. The competition between the brittle and ductile modes of failure has been intensively studied by Kalthoff and Winkler[3], Needleman [4], Kalthoff [5] and Ravi-Chandran [6] and found if the thermal softening rate (which depends upon loading rate) is sufficiently high, a transition from a brittle failure mode at low loading rates to a ductile failure mode at high loading rates occurs. Also the dynamic deformation and ASB propagating was measured in this ductile failure mode, i.e. Mason, Rosakis and Ravi-chandran [7], Zhou, Rosakis, and Ravi-chandran [8, 9].

In this study, the explosive loading experiments are performed on AISI 1020 steel tubes. Based on instability analysis of a thermoplastic constitutive relation, the strain-rate-dependent failure criterion is proposed to account for crack propagation and fracture mode transition. The dynamic crack growth and bifurcation are reproduced by finite element simulation using LS-DYN, and the result shows a good agreement with experiments.

2 Experiments

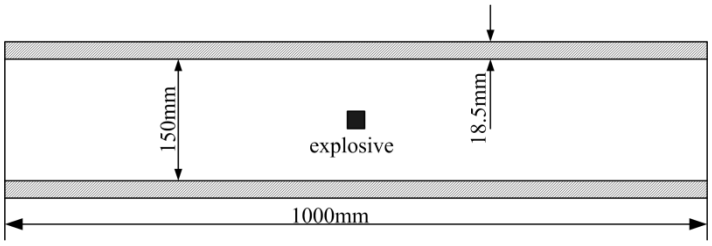

Fig.1 Structural size of the tube

The two AISI 1020 steel tubes with length of 1000mm, inner diameter of 150mm and thickness of 18.5mm are studied under the different explosion loads. Figure 1 shows the diagrammatic sketch of the cylinders, where the high explosive (HE) charges TNT are pressed into a hollow cardboard tube and located on the middle of the longitudinal axis of the tube. The tube was applied with increased charge sizes (250g, 425g and 600g) of TNT until to rupture.

3 Fracture analysis model

The decoupled method is used in the fracture analysis, where the calculated overpressures in ALE (Arbitrary Lagrangian-Eulerian) model (as depicted as $q(z,t)$ in figure 2) are applied on the inner surface of the cylinder as force boundary conditions. Using this method, the fluid-solid interactive effect is ignored to greatly decrease the computation cost and to guarantee the computation going smoothly. The length (l), inner diameter (D) and thickness (t) of the tube in fracture analysis model is as the same as experiments, however the initial crack size of $2a$ and $2b$ are allowed vary in a certain range. The finite element model in figure 2 shows the mesh around the crack. It has been found [10] that the explosive load rises to the maximum in dozens of microseconds, and the overpressure wave decay rapidly during this time, while fluid-solid interaction usually takes effects in a longer time scale such as the order of milliseconds. In the next sections, it will be proved the crack propagation also accomplished in the scale of microsecond. Therefore it is reasonable to ignore fluid-solid interaction and employ a decoupled method.

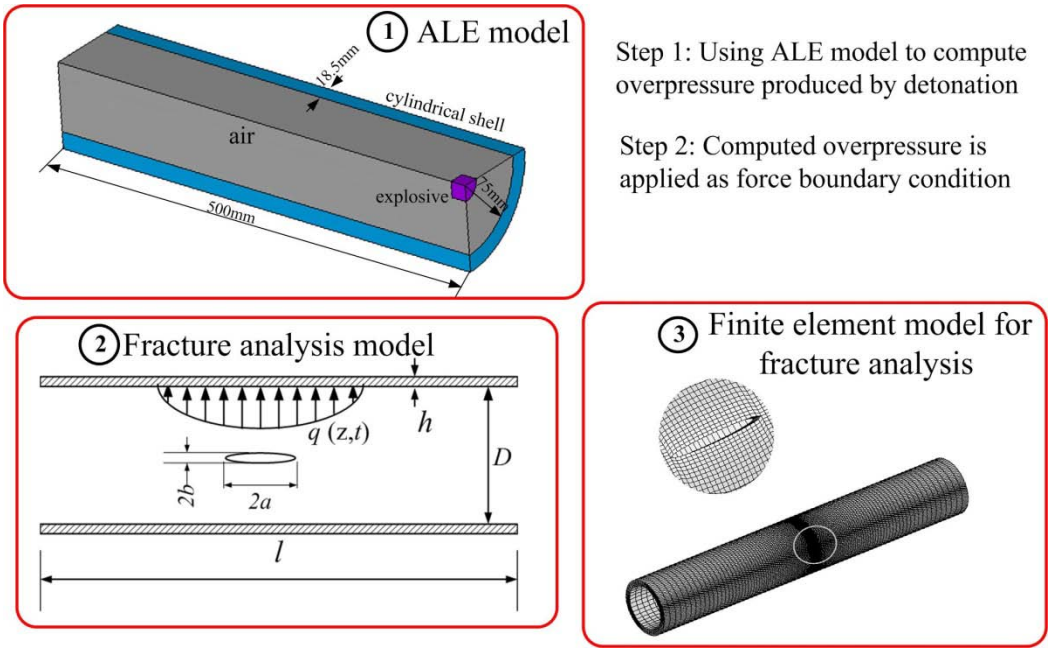

Fig.2 Fracture analysis procedure

4 Failure criterion

The material in the shear band experiences intensively localized shear deformation during high speed deformation, where the temporal scale of deformation is much shorter than that of heat conduction, and most of the heat transformed from the

inelastic energy stays inside the shear band, thus the process is approximately adiabatic and the shear band is nominated as adiabatic shear band (ASB). The phenomenon is frequently found during high strain rate deformation such as ballistic impact, explosive loading, high-speed shaping and forming, etc. A series Johnson-Cook type constitutive relations have been developed to describe such material behavior, and based on the instability analysis of the constitutive relation as Equation (1), a rate-dependent failure criterion is proposed to account for such damage mode.

$$\tau = (\tau_0 + E_1\gamma)(1 + g\ln\frac{\dot{\gamma}}{\dot{\gamma}_0})(1 - \alpha\frac{T}{T_0}) \tag{1}$$

where τ is shear stress, γ is shear strain, $\dot{\gamma}$ is shear strain rate, and T is temperature, T_0 and $\dot{\gamma}_0$ are reference temperature and reference strain rate, respectively. An instability analysis is conducted based on Equation (1), considering heat conduction and adiabatic condition, a rate-dependent failure criterion is obtained as Equation (2):

$$(1 + g\ln\frac{\dot{\gamma}_0}{\gamma_0})(A - \frac{\alpha\beta E_1}{T_0\rho c}\gamma)(\frac{\tau_0}{E_1} + \gamma) = 1 \tag{2}$$

The material parameters is given in Table 1 and the detailed derivation can be referenced [11].

Figure 3 shows the rate-dependent failure criterion represented by equation (2), where the critical strain decreases with the increment in strain rate, which is compatible with experimental observation that at higher strain rates deformations localize and materials fail at lower levels of plastic strains.

Table 4 Material parameters of steel tube

g	3.5×10^{-2}
τ_0	1060
E_1(MPa)	740
$\alpha/T_0\ (1/K)$	1.68×10-3
$\rho(g/cm^3)$	7.85

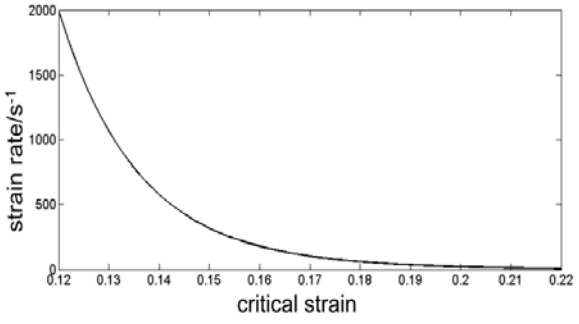

Fig. 3 Rate-dependent failure criterion

5 Results

The transient failure procedure is simulated by LS-DYNA, where the rate-dependent failure criterion represented by equation (2) is introduced into numerical algorithm. When the critical conditions are satisfied, the stress collapses and the corresponding

elements are removed, and thus the path formed by the removed material can approximately simulate the propagation of cracks.

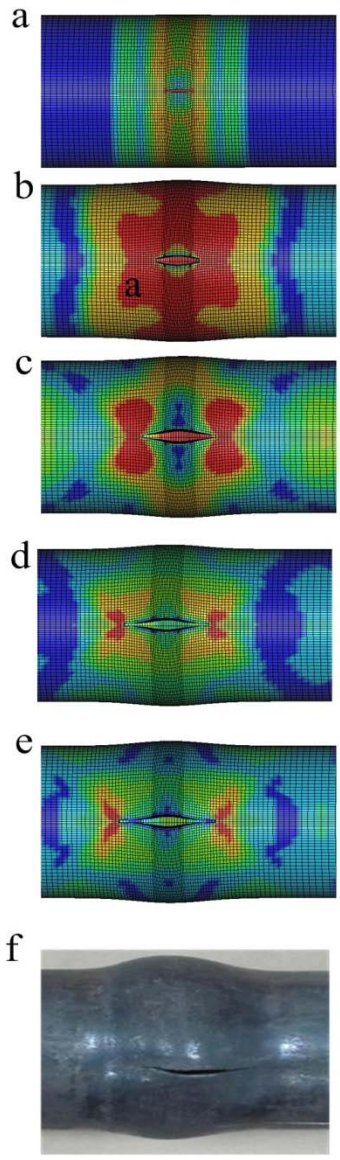

Fig. 4 Crack propagation with 425g TNT: a)t=25μs, b) t=85μs, c) t=265μs, d) t=735μs, e) t=1660μs f) experimental

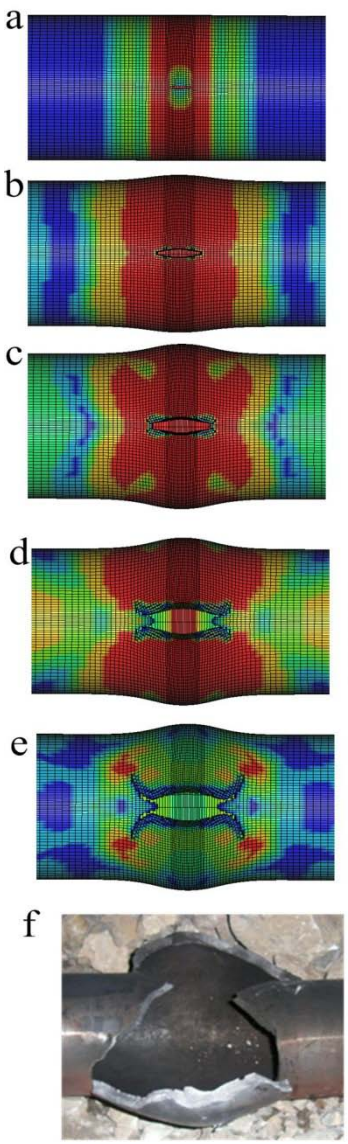

Fig. 5 Crack propagation with 600g TNT: a)t=25μs, b) t=70μs, c) t=105μs, d) t=885μs, e) t=1660μs f) experimental fracture mode

Figure 4 gives the effective stress distribution with crack propagation, where the explosive load is 425g TNT and the initial crack size is a=1.5cm and b=0.2cm. During the crack propagation, the crack opening displacement (COD) is found vibrates with structure breathing mode and the maximum COD is about 1.8 cm.

Figure 5 shows the crack propagation with the same initial crack size however explosive loading of 600g TNT. It is found that with the increment of load, the crack propagation mode and the final fracture profile begin to change significantly. The crack firstly extends longitudinally and from105 μs to 180 μs, it starts to bifurcate along the spiral line of the cylinder.

The cracking length histories with explosive loading of 425g TNT are depicted in figure 6, where the maximum cracking length is 5.62cm. The motion of the representative point which locates on the middle of the cylinder and 180 degree away from the location of crack center is chosen to illustrate the vibration of the cylinder. It is found that the crack propagation is compatible with the feature of vibration of structure, where most cracking length is accomplished during the first vibration period within 200 microseconds. When structure enters oscillation period, the cracking speed quickly slows down with a low crack length growth. Figure 7 gives the crack propagation history under 600g TNT. The total crack propagation length consisting of longitudinal axial crack length and spiral direction crack length reaches to 9.64cm, and nearly 80% crack length is accomplished during the first vibration period. All of crack histories indicate that crack mainly propagates during the first vibration period which depends upon the first impulse of pressure of load, and the followed structure oscillation has no obvious influence on the crack propagation.

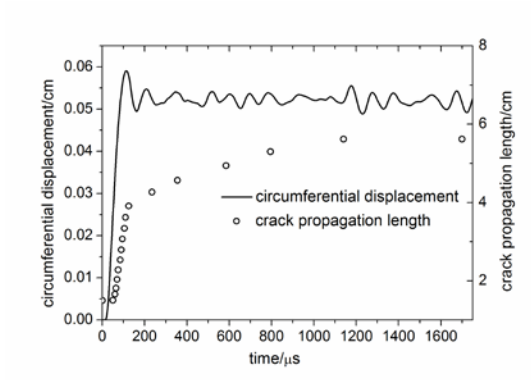

Fig.6 crack propagation with 425g TNT

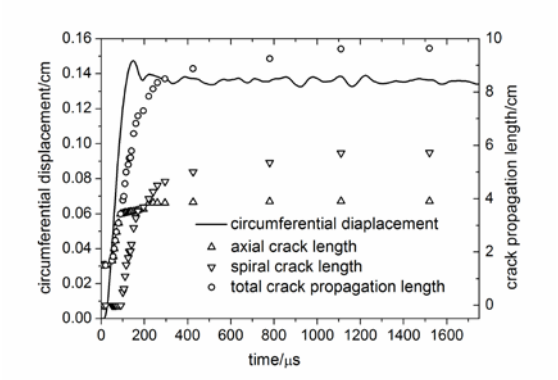

Fig.7 crack propagation with 600g TNT

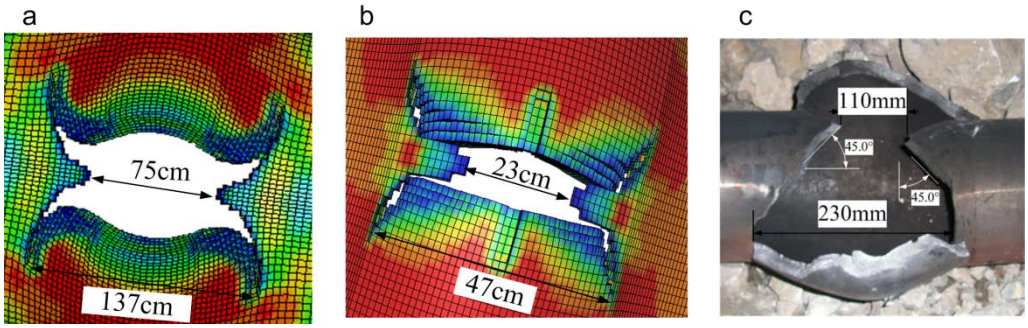

Fig.8 Fracture profile

Fig. 8 shows the simulated fracture with different initial crack shape and size under 600g TNT, where Fig.7 (a) is the result of initial crack size of a=3.0cm and b=0.45cm, and Fig.7 (b) is the result of embedded cross-shape initial-flaw with length of 1cm. Fig.15 (c) gives the experimental fracture profile under 600g TNT. The simulated result shows a good agreement with experiment. The comparison implies that the larger initial crack size leads to larger feature size of fracture, and the small-scale variation of initial crack shape and size does not cause obvious difference in final fracture mode under a given load condition. Also it should be acknowledged the difference of feature size of fracture between simulation and experiment. In fact, the

high-pressure air will release from the cracks and thus enlarges the fracture area, however, this enlarging effect is not considered in this simulation.

6 Conclusions

This paper presents a failure assessment method for structures under explosive loading. The failure criteria are strain rate-dependent and numerical simulation is conducted to reproduce the crack propagation. It is found that crack lengths and speeds increase with the increment of explosive load and the final fracture mode is nearly depend upon the intensity of explosive load, as well as strain rates. A limited variation of initial size and shape of cracks has minor influence on final fracture profile. Fracture mode transition is observed when nominal strain rate exceeds a certain value, and simulated fracture profile shows a good agreement with experiment result.

Acknowledgements

This work is supported by National Natural Science Foundation of China (Grant No. 51005201, 51275455).

References：

[1] A. M. Clayton. Hydrodynamics research facility design methods used for AWE containment vessels. Welding Research Council Bulletin 2001, 56(11-12): 6-28.

[2] Cases of ASME Boiler and Pressure Vessels Code, case 2564-2, Section VIII , Division 3, New York, 2010.

[3] J.K.Kalthoff, S. Winkler, Failure mode transition at high rates of loading. Proceedings of the International Conference on Impact Loading and Dynamic Behavior of Materials (Edited by C.Y. Chiem, H.D.Kunze and L.W. Meyer), 1988, 43-56.

[4] A. Needleman, V. Tvergaard, Analysis of a brittle-ductile transition under dynamic shear loading, International Journal of solids and structures, 1995, 32(17/18): 2571-2590.

[5] J. F. Kalthoff, A. BÜrgel , Influence of loading rate on shear fracture toughness for failure mode transition, International Journal of Impact Engineering 2004, 30: 957-971.

[6] Ravi-Chandar K., On the failure mode transitions in polycarbonate dynamic mixed-mode loading, International Journal of Solids and Structures, 1995, 32: 925-938.

[7] Mason J.J., Rosakis A.J., Ravi-chandran G., Full field measurement of the dynamic deformation field around a growing adiabatic shear band at the tip of a dynamically loaded crack or notch, Journal of Mechanics and Physics of Solids, 1994, 42: 1679–1697.

[8] Zhou M., A. J. Rosakis, G. Ravichandran, Dynamically propagating shear bands in impact loaded prenotched plates-I. Experimental investigation of temperature signatures and propagation speed. Journal of mechanics and physics of solids, 1996, 44(6): 981-1006.

[9] Zhou M., G. Ravichandran, A. J. Rosakis, Dynamically propagating shear bands in impact loaded prenotched plates-II. Numerical simulations, Journal of mechanics and physics of solids, 1996, 44(6): 1007-1032.

[10]Li Ma, Yang Hu, Jinyang Zheng, Guide Deng Yongjun Chen, Failure analysis for cylindrical explosion containment vessels, Engineering Failure Analysis, 2010, 17: 1221 – 1229.